Erosional truncation of uppermost Permian shallow-marine carbonates and implications for Permian-Triassic boundary events

Jonathan L. Payne†
Department of Geological & Environmental Sciences, Stanford University, 450 Serra Mall, Building 320, Stanford, California 94305, USA

Daniel J. Lehrmann
David Follett
Margaret Seibel
Department of Geology, University of Wisconsin at Oshkosh, 800 Algoma Boulevard, Oshkosh, Wisconsin 54901, USA

Lee R. Kump
Anthony Riccardi
Department of Geosciences, 503 Deike Building, The Pennsylvania State University, University Park, Pennsylvania 16802, USA

Demir Altiner
Department of Geological Engineering, Middle East Technical University, 06531, Ankara, Turkey

Hiroyoshi Sano
Department of Earth and Planetary Sciences, Kyushu University, Fukuoka 812-8581, Japan

Jiayong Wei
Guizhou Geological Survey, Bagongli, 550005 Guiyang, China

ABSTRACT

On shallow-marine carbonate buildups in south China, Turkey, and Japan, uppermost Permian skeletal limestones are truncated by an erosional surface that exhibits as much as 10 cm of topography, including overhanging relief. Sedimentary facies, microfabrics, carbon isotopes, and cements together suggest that erosion occurred in a submarine setting. Moreover, biostratigraphic data from south China demonstrate that the surface postdates the uppermost Permian sequence boundary at the global stratotype section and truncates strata within the youngest known Permian conodont zone. The occurrences of similar truncation surfaces at the mass-extinction horizon on carbonate platforms across the global tropics, each overlain by microbial buildups, and their association with a large negative excursion in $\delta^{13}C$ further suggest a causal link between erosion of shallow-marine carbonates and mass extinction. Previously proposed to account for marine extinctions, the hypothesis of rapid carbon release from sedimentary reservoirs or the deep ocean can also explain the petrographic observations. Rapid, unbuffered carbon release would cause submarine carbonate dissolution, accounting for erosion of uppermost Permian skeletal carbonates, and would be followed by a pulse of high carbonate saturation, explaining the precipitation of microbial limestones containing upward-growing carbonate crystal fans. Models for other carbon-release events suggest that at least 5×10^{18} g of carbon, released in <100 k.y., would be required. Of previously hypothesized Permian-Triassic boundary scenarios, thermogenic methane production from heating of coals during Siberian Traps emplacement best accounts for petrographic characteristics and depositional environment of the truncation surface and overlying microbial limestone, as well as an associated carbon isotope excursion and physiologically selective extinction in the marine realm.

Keywords: extinction, carbonate platform, carbon cycle, microbialite, calcification.

INTRODUCTION

Mass-extinction events are commonly associated with sedimentary facies changes reflecting environmental and biological disruption. The end-Permian mass extinction, the most severe extinction event in the history of animal life (Erwin, 2006), is associated with abrupt changes in sedimentary facies. On land, cessation of coal deposition (Retallack et al., 1996), changes in paleosol composition (Retallack, 1999; Sheldon, 2006), and fluvial depositional styles (Ward et al., 2000) all indicate substantial biological and environmental shifts. In shallow-marine carbonate strata, the extinction horizon is associated with a shift from skeleton-rich to skeleton-poor sediments (Baud et al., 1997; Payne et al., 2006) and an abrupt transition from skeletal to microbial and oolitic depositional modes (Baud et al., 1997, 2005; Sano and Nakashima, 1997; Lehrmann, 1999; Kershaw et al., 2002; Lehrmann et al., 2003; Groves and Calner, 2004; Wang et al., 2005). The abrupt onset of microbial and oolitic deposition has been interpreted as a direct consequence of extinction, due to reduced animal grazing on microbial mats (Schubert and Bottjer, 1992; Lehrmann, 1999), decreased skeletal carbonate deposition (Baud et al., 1997; Ezaki et al., 2003), increased carbonate saturation of seawater (Kershaw et al., 2002; Heydari et al., 2003; Lehrmann et al., 2003), or a combination of these factors.

The stratigraphic coincidence of the lithofacies transition with an abrupt decrease in fossil

†jlpayne@stanford.edu

GSA Bulletin; July/August 2007; v. 119; no. 7/8; p. 771–784; doi: 10.1130/B26091.1; 5 figures.

diversity and abundance (Baud et al., 1997; Payne et al., 2006) and a negative carbon isotope excursion (Baud et al., 1989) suggests that the contact corresponds to the time of extinction, rather than reflecting a biostratigraphically significant depositional hiatus, and its characteristics may shed light on the causes of extinction. The abrupt lithological transition has been suggested to result from subaerial exposure (Sano and Nakashima, 1997; Heydari et al., 2001; Unal et al., 2003), submarine erosion (Kershaw et al., 2002), or submarine carbonate dissolution (Heydari and Hassanzadeh, 2003). However, detailed petrographic studies of the contact have been limited by outcrop quality (e.g., Kershaw et al., 2002) and diagenetic pressure dissolution creating stylolites at the contact (e.g., Baud et al., 2005). Consequently, the precise temporal and genetic relationships among lithological, paleontological, and geochemical observations are unresolved.

Herein we report comparative petrographic observations of the transition from fossiliferous preextinction strata to microbial limestones in south China, Turkey, and Japan, representing eastern Tethys, western Tethys, and Panthalassa, respectively (Fig. 1A). This report builds upon previous studies at each of these localities (Baud et al., 1997, 2005; Sano and Nakashima, 1997; Lehrmann, 1999; Lehrmann et al., 2003). Observations described herein suggest widespread but short-lived submarine carbonate erosion prior to deposition of microbial limestones. Our preferred explanation for the coincidence of erosion with mass extinction is a pulse of carbon release (as CO_2 or methane) sufficiently large and rapid to induce shallow-water carbonate dissolution. This hypothesis can account for preferential extinction of marine genera in higher taxa characterized by heavy calcification and limited elaboration of respiratory organs (Knoll et al., 1996; Erwin, 2006), as well as the postextinction interval of widespread abiotic and microbial carbonate precipitation. By comparison to calculations made for similar scenarios hypothesized for the Paleocene-Eocene Thermal Maximum (PETM) (Zachos et al., 2005) and in the near future (Archer et al., 1997; Caldeira and Wickett, 2003), widespread carbonate dissolution requires the release of at least 5×10^{18} g C in less (or much less) than 100 k.y.

RESULTS

South China

Geological Setting

The Nanpanjiang Basin of southern China is in the Yangtze plate, which was located in the equatorial eastern Tethys during Permian–Triassic time (Enos, 1995). The Nanpanjiang Basin contains several isolated carbonate platforms and is surrounded by the Yangtze Platform, a vast attached carbonate platform that extends across southern China. The isolated platforms contain Permian-Triassic (P-T) boundary sequences with microbialite units as thick as 16 m and covering >10,000 km^2 (Fig. 1B) (Lehrmann, 1999; Lehrmann et al., 2003). The Langbai, Heping, and Dawen sections are on the Great Bank of Guizhou and the Taiping section is on the Chongzuo-Pingguo Platform (Fig. 1B). The Great Bank of Guizhou developed on antecedent topography near the former Permian margin of the Yangtze Platform during a Late Permian deepening event that caused stepback of the Yangtze Platform margin and drowning of shallow-marine carbonates in a vast area surrounding the Great Bank. The Chongzuo-Pingguo Platform developed upon an uplifted fault block in the southern part of the basin (Lehrmann et al., 2007).

The Late Permian–Middle Triassic depositional histories of the Great Bank of Guizhou and Chongzuo-Pingguo Platform were addressed by Lehrmann et al. (1998, 2007). Further studies have addressed microbialite development, carbon isotope stratigraphy, and biotic recovery from the end-Permian extinction in greater detail (Lehrmann, 1999; Lehrmann et al., 2001, 2003; Krull et al., 2004; Payne et al., 2004, 2006). Facies development across the P-T boundary interval on the Chongzuo-Pingguo Platform parallels that on the Great Bank of Guizhou (Lehrmann et al., 2003). On both platforms, Upper Permian shallow-marine skeletal packstones are overlain by calcimicrobial framestone with lenses of molluscan grainstone containing rare brachiopods and echinoderms, microgastropod packstone, and thin, planar-bedded, poorly bioturbated micritic limestone (Fig. 2A) (Lehrmann et al., 2003).

The P-T boundary facies are nearly identical in the Langbai, Heping, and Dawen sections of the Great Bank of Guizhou. We investigated 45 m of Upper Permian strata in detail beneath the P-T boundary in sections on the Great Bank of Guizhou. Upper Permian strata are thick-bedded, medium to dark gray, cherty bioclastic limestones with a diverse biota of brachiopods, crinoids, rugose corals, sphinctozoan sponges, bivalves, gastropods, foraminifers, calcareous algae, and *Tubiphytes*. The bioclastic packstones also contain peloids, are consistently massive, lack hydrodynamic structures, and locally are mud poor with shelter and geopetal fabrics. Chert occurs as black nodules and silicified fossils. Changhsingian foraminifers (*Palaeofusulina* and *Colaniella*) are abundant in the upper 10 m of the Upper Permian skeletal packstones on the Great Bank of Guizhou (Fig. 2A) (Lehrmann et al., 2003). The uppermost skeletal packstone bed at the Dawen section on the Great Bank of Guizhou contains a conodont assemblage including *Hindeodus latidentatus*, *H. eurypyge*, *H. praeparvus*, *H. typicalis*, *and Clarkina carinata* (Fig. 2A; T. Beatty, 2006, personal commun.). This assemblage indicates an age in the uppermost *H. praeparvus* zone or, more likely, the *H. changxingensis* zone. The latter interpretation is indicated by the occurrence of *H. eurypyge*, which does not occur below bed 27a at Meishan (Jiang et al., 2007). The conodont assemblage at Dawen is associated with abundant fusulinid foraminifers, calcareous algae, articulate brachiopods, echinoderms, and *Tubiphytes*, demonstrating the persistence of a diverse and abundant biota into the *H. changxingensis* zone. *H. parvus*, the conodont whose first occurrence defines the base of the Triassic Period at the global stratotype section and point in Meishan, China (Yin et al., 2001), occurs within the basal meter of the microbialite (Fig. 2A; Lehrmann et al., 2003). Therefore, the contact between the skeletal packtone and microbialite is interpreted as the extinction horizon and is interpreted to be biostratigraphically complete. At the Taiping section, the occurrence of the conodont *H. latidentatus* likewise indicates a latest Changhsingian age of skeletal packstone beneath the microbialite, and the occurrence of *H. parvus* within the microbialite indicates an earliest Triassic age (Lehrmann et al., 2003).

Petrography

The contact between fossiliferous packstone containing Late Permian fossils and the overlying microbialite was not described in detail in previous studies (Lehrmann, 1999; Lehrmann et al., 2003) due to limited availability of laterally extensive, unweathered outcrops. Quarrying subsequent to the previous studies provided a fresh exposure at Langbai (Fig. 3A). The contact between skeletal packstone and microbialite is sharp, irregular, and truncational at Langbai, exhibiting as much as 10 cm of relief with occasional overhanging topography. Microbial carbonate is adhered to the truncation surface and was precipitated beneath overhangs within sheltered cavities (Figs. 3B, 3C). Thin sections of the surface illustrate that it truncates grains and cement only in the underlying beds (Figs. 3D, 3E), and does not coincide with stylolites. The truncation thus formed prior to the deposition of the microbialite.

Underlying bioclastic packstone beds contain interparticle porosity partly filled with micrite and lined with isopachous bladed and fibrous calcite cements (0.02–0.06 mm) followed by clear equant calcite (0.02–0.25 mm) that occluded remaining porosity. The truncation

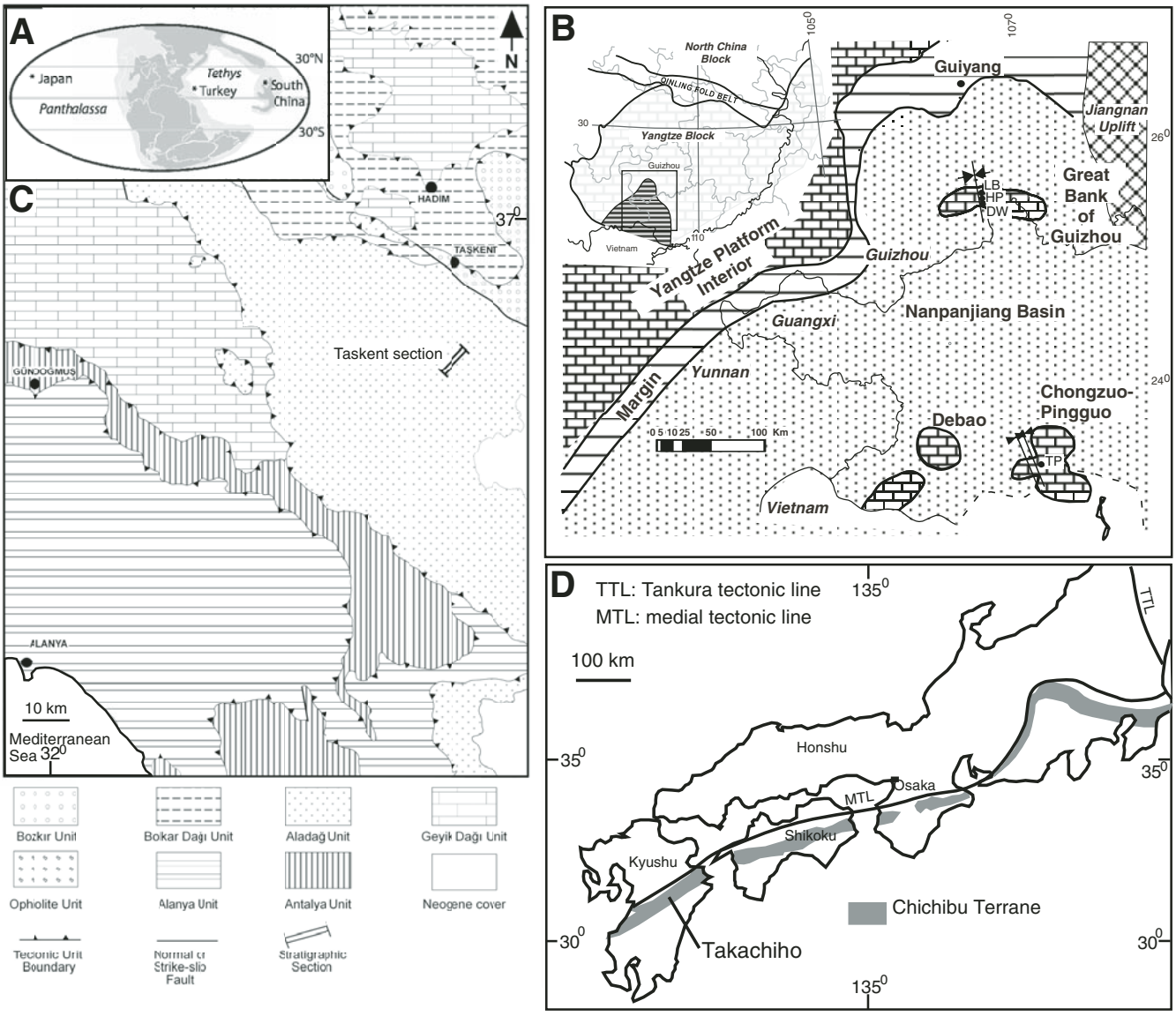

Figure 1. Permian-Triassic paleogeography and index maps for studied sections. (A) Paleogeographical reconstruction illustrating the positions of studied localities. Modified after Scotese (2005). (B) Index map for the Nanpanjiang Basin, south China, illustrating the positions of the Langbai (LB), Heping (HP), and Dawen (DW) sections on the Great Bank of Guizhou and the Taiping section (TP) on the Chongzuo-Pingguo Platform. (C) Index map for the Taşkent section, Turkey. (D) Index map for the Takachiho section, Japan. South China map modified from Lehrmann et al. (2003); Turkey map modified from MTA [General Directorate of Mineral Research and Exploration], 2002); Japan map modified from Ezaki and Yao (2000).

surface cuts fusulinids, other foraminifers, shell fragments, and peloids, as well as bladed and equant calcite cements. The skeletal packstones do not contain meniscus or pendent cements, vugs, or silt-filled dissolution voids or fractures. They also lack burrows and root casts. Samples taken across the packstone-microbialite contact in the Dawen section and near the Heping section contain a truncation surface nearly identical to the one described from Langbai.

On the Great Bank of Guizhou and at the Taiping section, the overlying microbialite unit consists primarily of a massive to digitate, thrombolitic framework of globular to lunate micrite-walled chambers and dense micrite clots. The occurrence of rare brachiopods and echinoderms within molluscan packstone lenses associated with the microbialite indicates deposition at normal marine salinity. The microbialite is overlain by thinly bedded, sparsely fossiliferous micritic limestone. Carbonate crystal fans as long as 1 cm are abundant near the base, but rare in the upper part of the microbialite unit (Fig. 3F). Crystal fans primarily radiate upward and contain growth bands indicative of multiple precipitation events. Some are nucleated on skeletal fragments or micrite clots and occur within primary cavities in the microbialite. At Taiping, crystal fans form the primary constructional framework at the base of the microbialite (Fig. 3F), indicating that the fans grew directly on the seafloor and produced upward-expanding digitate structures rather than forming within cavities in an existing microbial framework. The carbonate crystal fans are radial, fibrous, have square-tipped terminations, and are extensively

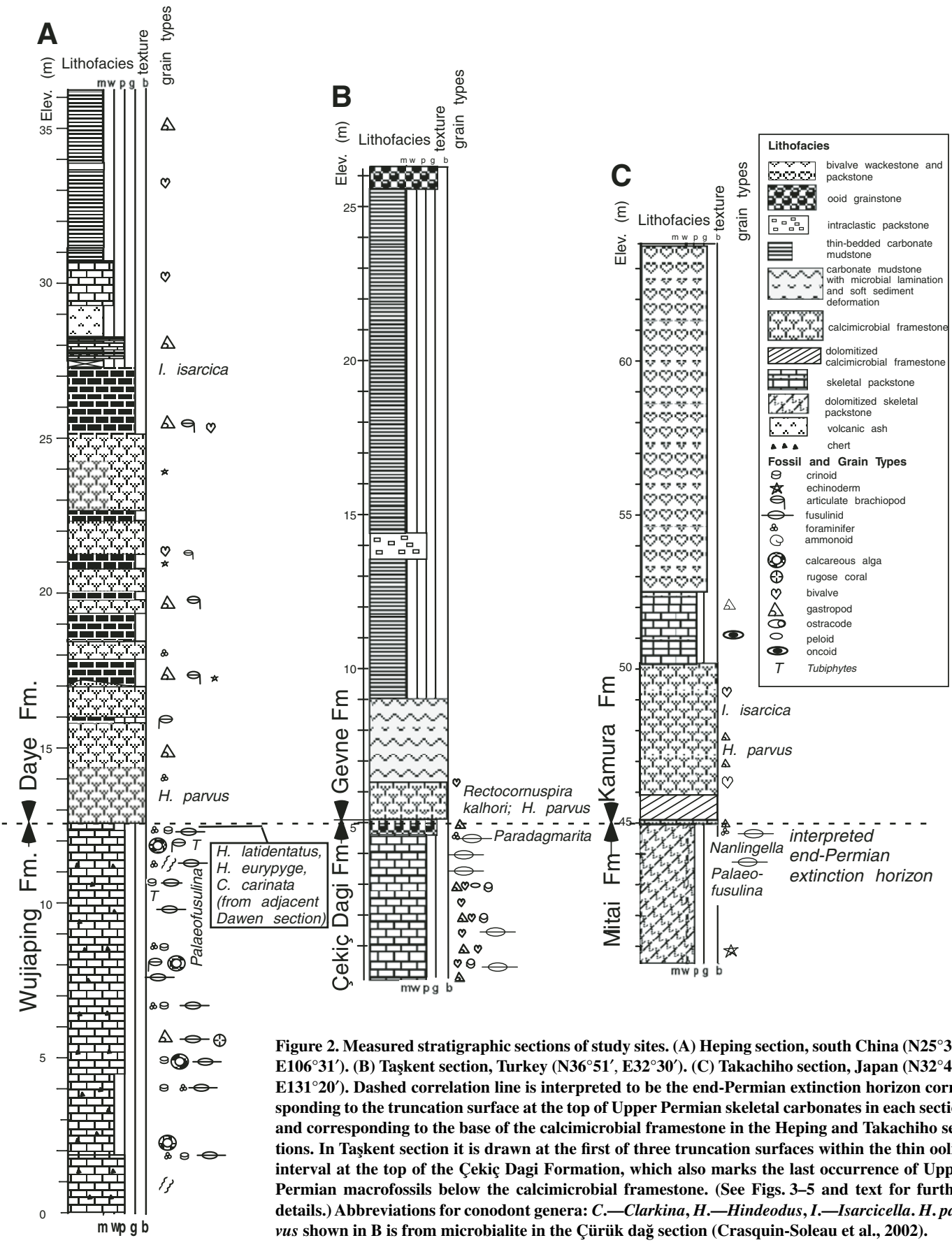

Figure 2. Measured stratigraphic sections of study sites. (A) Heping section, south China (N25°31′, E106°31′). (B) Taşkent section, Turkey (N36°51′, E32°30′). (C) Takachiho section, Japan (N32°45′, E131°20′). Dashed correlation line is interpreted to be the end-Permian extinction horizon corresponding to the truncation surface at the top of Upper Permian skeletal carbonates in each section and corresponding to the base of the calcimicrobial framestone in the Heping and Takachiho sections. In Taşkent section it is drawn at the first of three truncation surfaces within the thin oolite interval at the top of the Çekiç Dagi Formation, which also marks the last occurrence of Upper Permian macrofossils below the calcimicrobial framestone. (See Figs. 3–5 and text for further details.) Abbreviations for conodont genera: *C.—Clarkina*, *H.—Hindeodus*, *I.—Isarcicella*. *H. parvus* shown in B is from microbialite in the Çürük dağ section (Crasquin-Soleau et al., 2002).

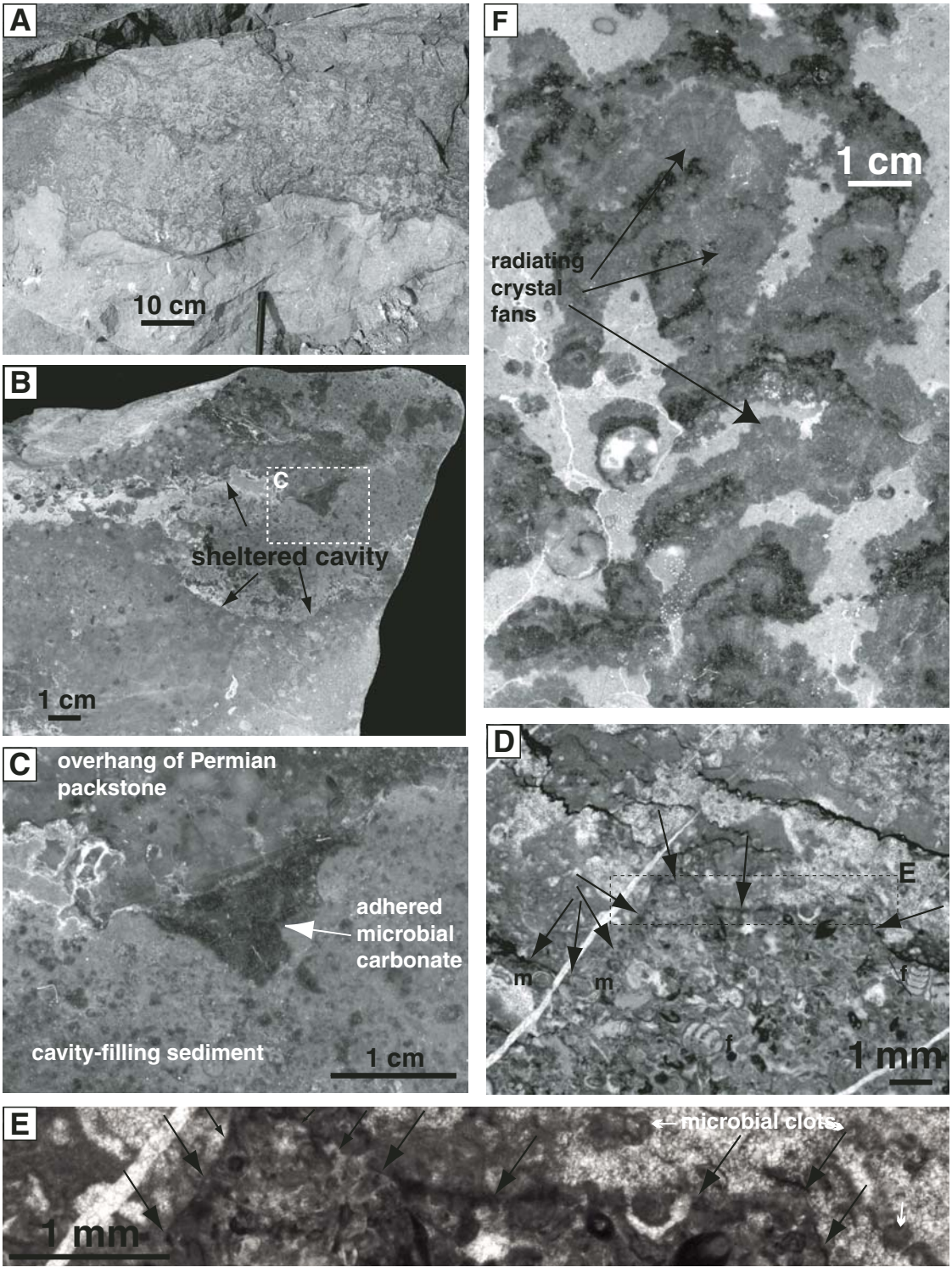

Figure 3. Illustrations of Permian–Triassic lithologies from south China. (A) Outcrop photo of irregular contact between fossiliferous Upper Permian grainstone (light gray) and microbialite (mottled dark gray) at Langbai. (B) Polished slab from Langbai illustrating overhanging topography on the Permian-Triassic boundary contact and microbialite adhered to overhanging Upper Permian limestone. Arrows indicate truncated contact between fossiliferous Permian packstone and postextinction sediment-filled cavity. (C) Detail of B. (D) Photomicrograph of truncational contact between fossiliferous packstone and microbialite (m) at Langbai. Permian foraminifers (*Cribrogenerina* sp.) are indicated (f), with one specimen cut by the truncation surface. Arrows indicate the position of the contact, which does not coincide with stylolites. (E) Detail of D, illustrating truncation of fabric in underlying bed. Arrows indicate the contact between fossiliferous packstone and the base of the microbialite. (F) Polished slab of basal microbialite at Taiping illustrating framework of upward-radiating carbonate crystal (aragonite) fans (medium gray), void-filling micrite (light gray), and microbial micritic clots (black).

recrystallized, suggesting an originally aragonitic mineralogy. Similar thrombolitic microbial mounds occur within younger Early Triassic strata on the Great Bank of Guizhou (Lehrmann, 1999; Lehrmann et al., 2001). Reexamination of these younger microbialites confirms that they consist exclusively of a clotted, micritic framework lacking crystal fans.

Interpretation of Depositional Environment

Changhsingian strata contain a diverse shallow-marine biota including fusulinids, calcareous sponges, echinoderms, and *Tubiphytes*. Fragmented skeletal grains and local mud-poor packstones indicate occasional wave agitation, whereas the lack of hydrodynamic structures, massive character, thick bedding, and mud-rich texture indicates relatively low energy conditions and perhaps bioturbation. The combination of observations indicates an open-marine subtidal setting above storm wave base.

Neither platform contains evidence of subaerial exposure within the Changhsingian strata. Beds underlying the truncation surface do not contain meniscus or pendent cements, vugs or moldic pores, or silt-filled dissolution voids. They also lack root casts, alveolar structures, burrows, and evidence of in situ brecciation of underlying beds. The 45 m of limestone below the truncation surface record continuous open-marine subtidal sedimentation without evidence of shoal facies or peritidal cycle development. There is no evidence of highstand systems tract or sequence development in the Upper Permian of these sections. The uppermost skeletal packstone beds and the truncation surface on the Great Bank of Guizhou postdate the sequence boundary at the Meishan section (Yin et al., 2001; Jiang et al., 2007), and all conodont zones are present. Together, these features suggest that the truncation surface at the top of the Changhsingian packstone formed by erosion and/or omission in a submarine environment, rather than erosion during subaerial exposure. The occurrence of a negative carbon isotope excursion above, rather than below, the truncation surface further supports erosion in submarine rather than subaerial conditions.

The occurrence of brachiopods and echinoderms within grainstone lenses in the overlying microbialite indicates that open-marine shallow subtidal conditions continued into the earliest Triassic. The absence of boring into the truncation surface suggests rapid deposition of microbial carbonates following erosion and/or low abundance of bioeroding organisms. If subaerial exposure had occurred in the Permian–Triassic succession of the Great Bank of Guizhou or Chongzuo-Pingguo Platform, it would necessarily have occurred abruptly and briefly within a substantial interval represented by open-marine conditions and left no diagnostic lithological signature. Therefore, we interpret the truncation surface in southern China to reflect omission and erosion in a submarine environment.

Turkey

Geological Setting

The Taşkent section occurs within the Aladag nappe, an allochthon thrust south over the autochthonous series of the Tauride block during the Eocene (Monod, 1977; Özgül, 1997) (Fig. 1C). Taşkent strata were deposited within the interior of a vast shallow-marine carbonate platform developed on the Tauride block in the western limits of the Tethys seaway during the Permian and Early Triassic (Marcoux and Baud, 1986; Groves et al., 2005).

The Taşkent section is >1 km thick, consisting of shallow-marine carbonate and siliciclastic strata of Late Permian–Middle Triassic age (Fig. 2B). Packages of shale and sandstone indicate that the carbonate platform was attached to land. Upper Permian strata of the Çekiç Dagi Formation are exclusively limestone and contain diverse marine fossils. We examined 50 m of the Upper Permian strata in detail; they consist of medium to thickly bedded, nodular limestones with packstone and wackestone texture, and exhibit burrow mottling, and contain a diverse biota of foraminifers, fusulinids, articulate brachiopods, echinoderms, gastropods, bryozoans, and calcareous algae. A Changhsingian age is indicated by the biseriamminid foraminiferan *Paradagmarita monodi* (Fig. 2B; Groves et al., 2005). Additional foraminifers include lagenids, hemigordiopsids, staffelids, and other biseriamminid foraminifers (Groves et al., 2005). The fossils, muddy texture, bioturbation, and lack of hydrodynamic structures in this unit indicate deposition on a moderately deep, open-marine, subtidal platform, except for high-energy subtidal conditions indicated by oolite grainstone in the uppermost 20 cm of the formation (Fig. 2B).

Overlying the Çekiç Dagi Formation is the Triassic Gevne Formation, which contains microbialites in its basal part (Fig. 2B). Occurrences of the early Griesbachian foraminifer *Rectocornuspira kalhori* in the microbialites (Unal et al., 2003) place the P-T boundary near the contact between the two formations (Fig. 2B). Occurrence of the conodonts *Hindeodus parvus* and *Isarcicella isarcica* in the stratigraphically equivalent microbialites of the Çürük dağ section also support a basal Griesbachian age (Crasquin-Soleau et al., 2002). A gradual decline in $\delta^{13}C$ from 4‰ to 2‰ in the upper 2 m of the Çekiç Dagi Formation at Taşkent (Richoz, 2004) suggests an uppermost Changhsingian age for these strata and P-T boundary position near the top of the formation by comparison to the carbon isotope stratigraphy of Meishan (Jin et al., 2000).

Petrography

The top of the Çekiç Dagi Formation is marked by a 20-cm-thick oolitic unit (Fig. 2B). The lower 10 cm of this horizon is a bioclastic grainstone composed mainly of well-rounded, sand-sized, unidentifiable fossil fragments, calcareous algae, a variety of foraminifers including the Changhsingian foraminifer *Paradagmarita*, and rare echinoderms (Fig. 4A). Rounded grains that appear to be ooids in outcrop are often revealed in thin section to be well-rounded skeletal grains

Figure 4. Illustrations of Permian–Triassic lithologies from Taşkent, Turkey. (A) Photomicrograph illustrating calcareous algae (a), rounded skeletal grains, and unidentifiable, recrystallized grains in the bioclastic grainstone below the Permian-Triassic (P-T) boundary. (B) Photomicrograph illustrating recrystallized ooids from a few centimeters below the base of the microbialite. (C) Photomicrograph of gastropod-bearing oolitic limestone, illustrating recrystallized ooids (o), silt-sized quartz grains (q), gastropods (g), and an echinoderm fragment (e). (D) Photomicrograph of gastropod-bearing oolitic limestone, illustrating silt-sized quartz (q), isopachous fibrous calcite cement (f), and sparry calcite cement (s). (E) Polished slab of P-T boundary at Taşkent illustrating the sharp contact between oolite and clotted microbialite as well as transition to layered microbialite. Three truncation surfaces are indicated by partial tracings with dashed lines. The uppermost truncation surface indicated marks the contact between the oolitic unit and overlying clotted microbialite. (F) Photomicrograph (reflected light) of the P-T boundary illustrating truncated ooids (o). Surface corresponds to uppermost truncation surface indicated in E. Aragonite fans grow from the surface and are overlain by clotted microbial framework. Gastropod shells (g) are also indicated. (G) Photomicrograph of P-T boundary illustrating concentration of fine quartz grains immediately underlying the base of the microbialite above a sharp truncation surface (arrows) with underlying, quartz-bearing oolite. The indicated surface corresponds to the uppermost truncation surface indicated in E.

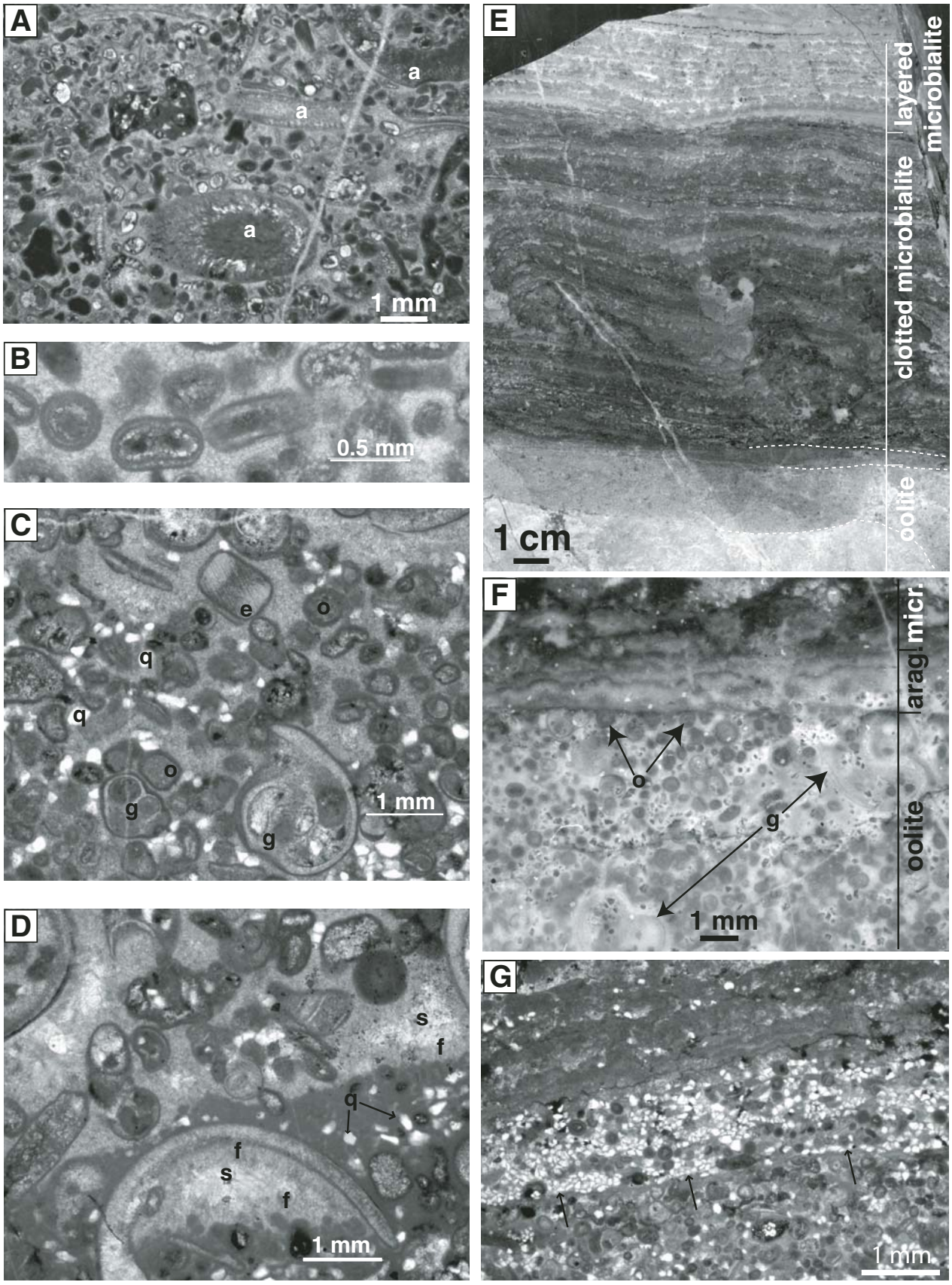
A
a
a
a
1 mm
B
0.5 mm
C
e
o
q
q
o
g
g
1 mm
D
s
f
q
f
s
f
1 mm
E
layered microbialite
clotted microbialite
oolite
1 cm
F
arag. micr.
o
g
oolite
1 mm
G
1 mm

or superficial ooids (Figs. 4A–4C). Isopachous bladed cements 0.10–0.25 mm thick encrust the ooids and skeletal grains, followed by clear, equant calcite cement that occludes remaining porosity (Fig. 4D). The bioclastic grainstone is terminated by a sharp truncation surface overlain by 10 cm of oolitic skeletal grainstone with admixed fine quartz sand. The truncation surface is the lowest of the three truncation surfaces illustrated in Figure 4E. This upper oolitic-skeletal grainstone lacks diagnostic Permian fossils and contains rare echinoderms and abundant gastropods up to a few millimeters in maximum dimension (Figs. 4B–4D). Ooids within this unit were not observed to nucleate on co-occurring quartz grains. The uppermost truncation surface is illustrated in reflected and transmitted light in Figures 4F and 4G, respectively. Ooids are largely replaced by equant sparry calcite but are not compacted, indicating that replacement occurred after burial rather than during early diagenesis (Figs. 4B–4D). Each erosion surface truncates ooids, gastropods, and cements.

The uppermost truncation surface at the top of the oolitic interval is encrusted directly by radiating fibrous carbonate crystal fans in some samples (Fig. 4F), and a lag deposit of silt-sized quartz and ooids overlain by microbial limestone in others (Fig. 4G). Quartz-ooid lag deposits appear to be concentrated in local topographic low points on the truncation surface, and are enriched in quartz relative to underlying sediments. Microbialite immediately overlies the crystal fans above the truncation surface at the top of the oolitic interval (Figs. 2C and 4E–4G). The base of the microbialite is a thrombolitic, mounded biostrome, 10–20 cm thick, built by irregular micritic clots and containing constructional voids as much as 2 cm high filled with micritic sediment, ostracods, gastropods, and foraminifers (Fig. 4E). The clotted framework varies from chambers bordered by micrite to solid micritic clots of similar dimensions. Radiating carbonate crystal fans encrust the microbial framework. The mounded biostrome is overlain by a 1 m interval of micrite clots in discrete layers rather than mounds (Fig. 4E). Bladed isopachous cements line voids between clotted layers. Overlying the layered micrite clots is 2.8 m of laminated to thinly bedded, unfossiliferous micrite exhibiting wavy bedding, possible stromatolitic mounds, microbial lamination, and soft-sediment folds (Fig. 2B).

Interpretation of Depositional Environment

Previous studies (Marcoux and Baud, 1986; Baud et al., 1989; Unal et al., 2003; Groves et al., 2005) interpreted the oolitic interval to represent a subaerial exposure surface, but did not provide detailed petrographic observations to support this interpretation. Our investigation revealed no diagenetic fabrics definitive of subaerial exposure (e.g., meniscus or pendent cements, vugs, or large silt-filled voids) (Hillgartner, 1998; Immenhauser et al., 1999; Sattler et al., 2005). The carbon isotope composition of the oolites is heavier than that of the overlying microbialite (Richoz, 2004), contrary to observations of other exposure surfaces on carbonate platforms (Immenhauser et al., 1999). Cementation by bladed isopachous calcite cements within the oolite, and the absence of pendent or meniscus cements, instead suggests marine phreatic conditions. Ooids replaced by equant calcite spar in this unit resemble ooids leached by subaerial diagenesis; however, the lack of compaction, dropped nuclei, or internal sediment within the ooids suggests replacement after burial rather than dissolution during early diagenesis. Thus, we interpret the truncation surfaces within the upper 10 cm of the Çekiç Dagi to have formed by submarine omission and/or erosion.

Our interpretation does not necessarily contradict the interpretation of Unal et al. (2003), that the oolite at the top of the Çekiç Dagi Formation at Taşkent is equivalent to Wignall and Hallam's (1992) first punctuated aggradational cycle of the P-T boundary interval at Tesero (Italy), with the second aggradation cycle missing in the Taşkent area. If the Unal et al. (2003) correlation is correct, it merely suggests that erosion in the Taşkent area occurred in a submarine setting, rather than during subaerial exposure. However, similar to the case in southern China, the upper 50 m of Upper Permian strata at Taşkent are entirely subtidal and lack any peritidal cyclicity indicative of highstand or sequence boundary development leading up to the oolite and truncation surfaces. Of course, this interpretation does not rule out the possibility that other regions on the same carbonate platform underwent subaerial exposure.

Baud et al. (2005) suggested that the truncation surface and concentration of silt-sized quartz at the contact between the oolite and microbialite formed during diagenetic pressure dissolution. Such is clearly the case in their illustrated sample (their Fig. 4D), but our examination of multiple slabs and thin sections from Taşkent reveals that stylolites are not ubiquitous at this contact. Our samples clearly demonstrate early, syndepositional truncation and sedimentary lag concentrations of silt-sized quartz underlying the base of the microbialite.

The basal Triassic microbialite unit is interpreted to have been deposited in shallow, open-marine subtidal environments, by analogy to the similar microbialites in southern China. The presence of marine phreatic cements and absence of vadose cements are consistent with shallow, open-marine deposition. However, definitive stenohaline taxa such as brachiopods and echinoderms have not been identified within the microbialite unit at Taşkent.

Japan

Geological Setting

The Takachiho section occurs in the Chichibu terrane of central Kyushu (Fig. 1D). It represents shallow-marine carbonate sedimentation on a Panthalassic seamount that was tectonically embedded into the Jurassic subduction-generated accretionary complex of southwest Japan. The geologic setting, facies, and depositional setting of this section were described in detail by Sano and Nakashima (1997). The Takachiho section contains dolomitized skeletal wackestone-mudstone of the Upper Permian Mitai Formation overlain by Early Triassic calcimicrobial framestone in the base of the Kamura Formation and Early–Middle Triassic bivalve wackestone-packstone (Fig. 2C) (Sano and Nakashima, 1997). Kanmera and Nakazawa (1973) reported the fusulinid foraminifers *Nankinella*, *Staffella*, and *Codonofusiella* from the Upper Mitai Formation, indicating a Late Permian (middle Changhsingian) age. The presence of *H. parvus* and *I. isarcica* within the calcimicrobial framestone in the basal part of the Kamura Formation demonstrates a basal Triassic Griesbachian age (Koike, 1996; Sano and Nakashima, 1997).

The Mitai Formation is entirely composed of pervasively dolomitized, thickly bedded, skeletal-peloidal wackestone-mudstone. The lower part contains diverse foraminifers, crinoids, echinoids, gastropods, bivalves, *Tubiphytes*, and calcareous algae (Sano and Nakashima, 1997). The upper part of the Mitai Formation exhibits a gradual upward decrease in skeletal abundance and diversity. The basal 0.9 m of the overlying calcimicrobial framestone is also dolomitized (Fig. 2C). By analogy to sections in Turkey and China, we have placed the boundary between the Mitai and Kamura Formations within the dolomitized interval, at the contact between the wackestone containing Upper Permian fusulinids and overlying microbial carbonates (Fig. 2C).

Petrography

Dolomitization obscures the basal contact of the microbialite in outcrop at Takachiho. One dolomitized sample was determined, upon investigation of polished slab and thin section, to contain the contact between fossiliferous wackestone and the overlying microbialite. The contact exhibits vertical topography and sharply truncates underlying peloidal wackestone containing fusulinid and miliolid foraminifers (Figs. 5A, 5B). Crystal fans encrust the surface

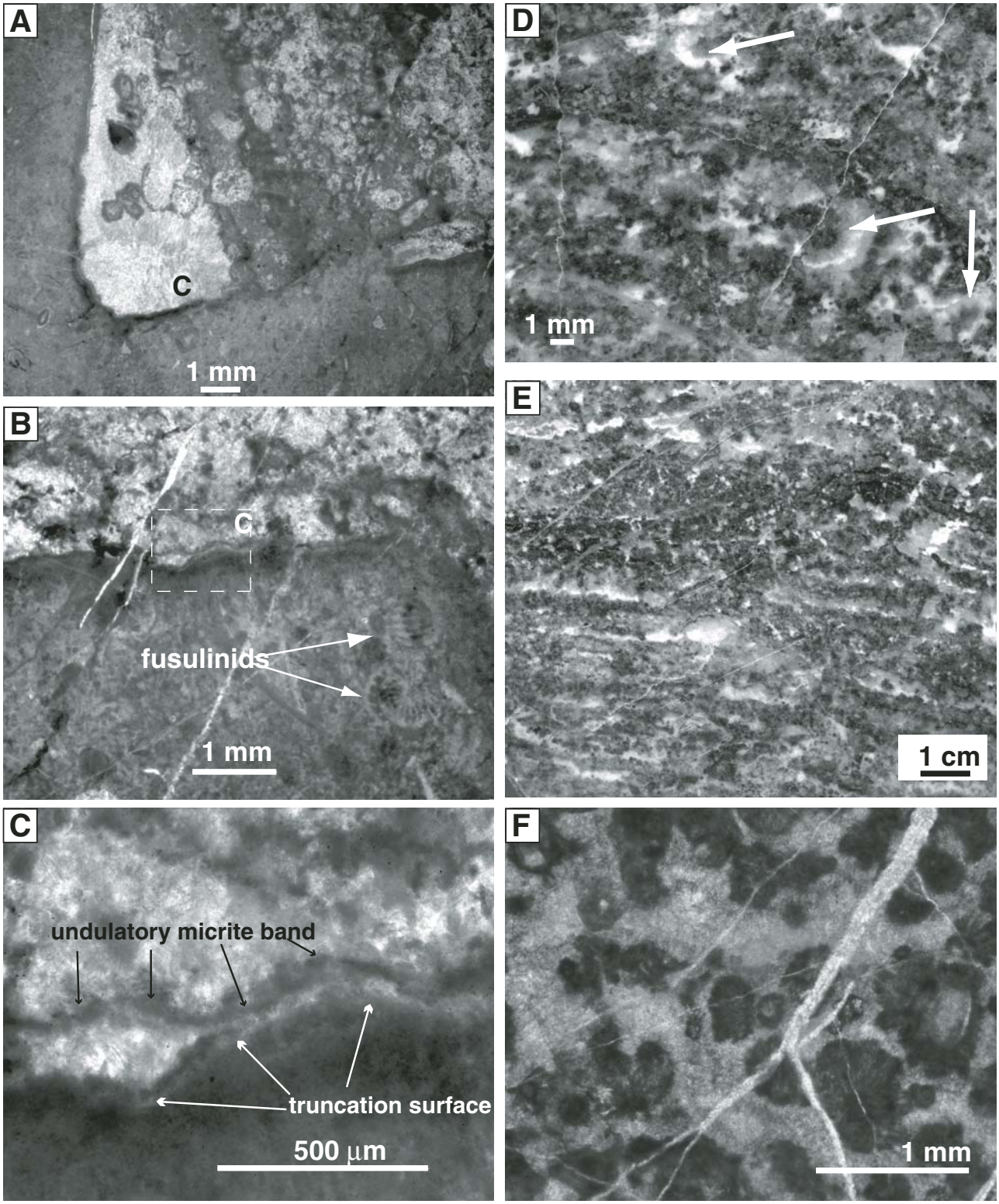

Figure 5. Illustrations of Permian–Triassic lithologies from Takachiho section, Japan. (A) Photomicrograph of the contact between peloidal wackestone and overlying microbialite. Note vertical contact on the left side of the figure and the crystal fans (c) developed immediately above the contact. (B) Photomicrograph illustrating two fusulinid foraminifers immediately underlying the truncation surface. (C) Detail of B, illustrating undulatory bands of micrite immediately overlying the truncation surface. (D) Polished slab of the microbialite illustrating clotted framework and abundant encrusting carbonate crystal fans (indicated by arrows). (E) Polished slab of the microbialite unit illustrating layering in the clotted framework. Note abundant fibrous cement and fans (medium gray) within cavities. (F) Photomicrograph of the microbialite illustrating dark micritic clots overgrown by radial fibrous cements.

in a sheltered cavity (Fig. 5A). The surface is not stylolitized (Figs. 5A, 5B), and is directly overlain by undulatory bands of micrite 10–20 μm thick (Figs. 5B, 5C) that may reflect the presence of microbial mats and/or cements growing on the truncation surface.

The microbialite framework consists of micrite-walled chambers and solid micritic clots locally encrusted with abundant carbonate fans (Figs. 5D–5F) (Sano and Nakashima, 1997). Micritic clots are cemented by 0.2–0.5 mm of fibrous calcite cement, followed by a similar thickness of clear, equant sparry calcite. In some samples, fibrous calcite cement completely occludes voids in the clotted framework and clear, equant calcite cement is absent (Fig. 5F). The uppermost 0.9 m of dolomitized strata was previously assigned to the Mitai Formation by Sano and Nakashima (1997), but contains clotted microbial framework. Aside from dolomitization, this interval is otherwise petrographically identical to the base of the overlying Kamura Formation as it was previously defined. Therefore, we interpret the contact between dolomitized skeletal wackestone and dolomitized microbialite to correspond with the similar lithological contact in south China. Dolomitization appears to be secondary in these strata, as supported by vertical and lateral patchiness of dolomitization in the base of the microbialite. Constructional voids in the microbialite are as much as 1 cm in maximum dimension and contain skeletal grains and fragments of the microbialite framework. Samples taken near the base of the microbialite that appear clotted in hand sample commonly consist primarily of radiating crystal fans growing from darker, micritic nuclei (Fig. 5D). As at other localities, the carbonate fans are fibrous and recrystallized, suggesting an originally aragonitic mineralogy.

Interpretation of Depositional Environment

Sano and Nakashima (1997) interpreted the uppermost Mitai Formation and the overlying microbial framestone to have been deposited in a tidal-flat environment. However, they also reported rare crinoids within the microbialite, indicating normal-marine salinity, and our further investigation has revealed the occurrence of fusulinid foraminifers in the uppermost centimeter of the skeletal wackestone. Vertical and lateral patchiness of dolomitization over a few decimeters, its persistence across the lithological contact between fusulinid-bearing wackestone and microbialite, and coarsely crystalline texture in many samples indicate that it occurred during burial diagenesis and is unlikely to reflect evaporative, intertidal depositional conditions. Moreover, fusulinids are indicative of normal marine environments, rather than evaporative intertidal settings (Flügel, 2004). Therefore, although changes in fossil abundance and composition within the Mitai Formation indicate upward shallowing, we interpret the uppermost beds to have been deposited in an open-marine, shallow subtidal environment.

DISCUSSION

Permian–Triassic Depositional Events

Similar patterns of carbonate deposition and erosion occur across the P-T boundary in south China, Turkey, and Japan. Upper Permian skeletal carbonates are abruptly overlain by microbialite containing earliest Triassic conodonts and lacking diagnostic Permian fossils. In south China, the uppermost skeletal packstone beds are biostratigraphically younger than the uppermost sequence boundary interpreted at the intensively studied Meishan section. The ages of the beds immediately underlying the truncation surfaces at the Turkish and Japanese sections are not as well defined, but correspondence of lithological and carbon isotope data suggests similar stratigraphic completeness.

Biostratigrapic completeness does not rule out subaerial exposure between skeletal and microbial carbonate deposition. Truncation surfaces can be developed on carbonate platforms during intervals of subaerial exposure, submarine omission, and submarine erosion. Distinguishing subaerial and submarine scenarios is difficult because subaerial exposure does not always leave diagnostic lithological evidence and, when it does, such evidence may be removed by subsequent submarine erosion (Immenhauser et al., 1999; Sattler et al., 2005). Lithological and geochemical observations of the studied sections provide no positive evidence for exposure and are consistent with erosion in a submarine environment. Facies underlying the surface are subtidal, rather than intertidal, and there are no shallowing-upward cycles to indicate highstand systems tract or sequence development. Isopachous cements lining voids indicate marine phreatic cementation. Vugs and meniscus or pendent cements indicative of exposure and meteoric diagenesis have not been observed at any of these sites. Thus, the truncation surface lacks most or all of the features commonly associated with subaerial exposure on carbonate platforms (Hillgartner, 1998; Immenhauser et al., 1999; Sattler et al., 2005). Similarly, the presence of stenohaline taxa within the skeletal carbonates at all three localities and within the microbialite interval in south China and Japan indicates deposition within waters of normal marine salinity below and above the truncation surface. Cryptic exposure surfaces may be identified in some cases via the isotopically light carbon and oxygen isotope composition of underlying strata, acquired during meteoric diagenesis (Immenhauser et al., 1999; Sattler et al., 2005). In the case of the truncation surfaces addressed in this study, however, carbon isotope data universally reveal lighter values above the surface rather than below it (Musashi et al., 2001; Krull et al., 2004; Payne et al., 2004; Richoz, 2004).

The contact between skeletal packstone and microbialite in south China is younger than the sequence boundary interpreted to occur shortly before the mass extinction at Meishan and other localities. It is also biostratigraphically complete, suggesting that erosion did not remove a substantial thickness of sediment or corresponding time. Although biostratigraphic data cannot rule out the possibility that the truncation surface was developed earlier in Turkey and Japan than in southern China, lithological and geochemical correspondence among the sites suggests that strata underlying the surface are correlative. Moreover, the occurrence of *H. parvus* within the microbialite at all three localities confirms coeval deposition of the overlying strata. Therefore, if subaerial exposure occurred on these platforms, it occurred coincident with mass extinction and without leaving diagnostic petrographic or geochemical evidence. Consequently, we prefer to interpret the truncation surface as a submarine erosion surface developed at the time of extinction.

Similar depositional histories appear to characterize other P-T boundary strata in carbonate depositional systems. Heydari and Hassanzadeh (2003) suggested that submarine dissolution occurred at the Abadeh section in Iran on the basis of poor textural preservation of uppermost Permian beds, but did not illustrate an erosional surface (see also Heydari et al., 2003). In other localities, a boundary clay is present between fossiliferous Upper Permian strata and overlying microbialites (Baud et al., 1997; Haas et al., 2006). In the Sichuan basin of China, erosion below the base of the microbialite may be minimal (Kershaw et al., 1999). Kershaw et al. (2002) reported an absence of petrographic features diagnostic of subaerial exposure, but noted that outcrop quality of the contact was generally poor, preventing detailed analysis of the contact. At Meishan, China, Cao and Shang (1998) reported several burrowed surfaces within bed 27: they were able to correlate the lowest such surface, at the top of bed 27a, across all of the Meishan quarries and suggested that erosion by burrowing might have been enhanced by dissolution at this level. The surface exhibits as much as 3 cm of relief and is immediately overlain by small rock and shell fragments that appear to be derived from the underlying bed (Cao and Shang,

1998); however, they did not present photomicrographs or a detailed description of the surface. In contrast, they found that overlying burrowed surfaces could not be correlated among separate sections. Biostratigraphically, the level of widespread burrowing and possible dissolution at Meishan appears to correlate with the truncation surface on the Great Bank of Guizhou.

The precise timing of the main P-T boundary extinction pulse appears to vary slightly among sections when all fossil occurrence patterns are taken at face value. At Meishan, last occurrences of Permian fossils cluster at the top of bed 24e (Jin et al., 2000), whereas extinction on the Great Bank of Guizhou appears to be correlative with the top of Meishan bed 27a. In Hungary, extinction appears to have occurred immediately below or within the boundary shale that underlies the microbialite (Haas et al., 2006). Although such observations could indicate a diachronous extinction pattern, they could also reflect local lithofacies controls on fossil occurrences that result in offsets between last occurrences among sections and/or minor sampling- and facies-related offsets in conodont ranges. Because lithofacies variation, fossil abundance patterns, and sampling intensity can affect the precise arrangement of observed first and last occurrences for fossil species in any give stratigraphic section (Signor and Lipps, 1982; Holland, 1995), it is unlikely that last occurrences will correlate to the centimeter scale among widely separated sections representing differing tectonic settings and depositional environments. In this case, the deposition of shale at the boundary on attached carbonate platforms and carbonate ramps may also reflect reduced carbonate production and resulting concentration of siliciclastic sediments.

Explanatory Models

When each is taken in isolation, none of the lithological features associated with the P-T boundary in the carbonate platforms is unique to this interval. Truncation surfaces are common features on carbonate platforms, and many appear to occur without subaerial exposure (Hillgartner, 1998; Immenhauser et al., 1999; Sattler et al., 2005). Microbial mounds are common in the Phanerozoic geological record, both in isolation and in association with metazoan reef builders (Webb, 1996). Even crystal fans are common within Permian and Triassic reef carbonates (Grotzinger and Knoll, 1995; Flügel, 2002). What sets the P-T boundary interval apart is that the abrupt transition from skeletal to microbial and oolitic facies in carbonate platforms occurred across the global tropics and was coeval with a biotic crisis and a large carbon cycle perturbation. A satisfactory model of P-T boundary events should account for each of these features, as well as data from other sources.

Extinction

One possibility is that the truncation surface, overlying microbialite, and carbon isotope excursion are all consequences of extinction and do not directly reflect or require any particular extinction mechanism. Rampino and Caldeira (2005) suggested that collapse of primary productivity and the biological pump in the aftermath of the extinction could account for the negative carbon isotope excursion. They noted that this scenario would also produce a short-term decrease in the carbonate saturation of seawater as pCO_2 increased, followed by an interval of ~1 m.y. characterized by elevated carbonate saturation as silicate weathering responded to increased pCO_2. Under this model, erosion and truncation would occur immediately following mass extinction during the interval of reduced carbonate saturation, and microbialite deposition would follow during the interval of elevated silicate weathering.

Carbon Release via Upwelling

Some extinction models (e.g., Knoll et al., 1996; Kump et al., 2005) propose carbon transfer from the deep ocean to the surface ocean and atmosphere. As a result of the biological pump, deep waters are enriched in nutrients and CO_2 and surface waters are nutrient deficient and equilibrated with atmospheric CO_2 at much lower concentrations. Under typical circumstances, upwelling deep waters evolve to surface waters with minimal degassing, because biological uptake of CO_2 in excess of that in equilibrium with the atmosphere is supported by upwelling nutrients (e.g., Broecker and Peng, 1982). However, if those upwelling waters are toxic to most phytoplankton (Kump et al., 2005), or if biological productivity is otherwise unable to keep pace with upwelling (as might have occurred during biospheric crises, such as the end-Permian extinction), CO_2 degassing will take place, promoting intensive cementation on the outer shelf to slope at the site of upwelling and forcing atmospheric pCO_2 to rise globally. In areas far from upwelling zones, including inner shelf settings, equilibration with CO_2 accumulating in the atmosphere from degassing could cause local carbonate undersaturation. Such a model has been proposed to account for abundant seafloor fans in outer shelf sediments deposited late in the Early Triassic (Woods et al., 1999).

Carbon Release from Sediments

Other models propose carbon release from sediments to the atmosphere and oceans (Krull and Retallack, 2000; Erwin, 2006). Carbon release from sediments to the atmosphere would force the system globally, initially promoting widespread seafloor carbonate dissolution in all settings, and subsequently causing rapid carbonate deposition through accelerated silicate and carbonate weathering and resultant delivery of carbonate alkalinity to the oceans (Archer et al., 1997). Destabilization of methane clathrates on the seafloor (Krull and Retallack, 2000) and thermogenic methane production during interactions between Siberian Traps magmas and carbon-rich crustal strata (Svensen et al., 2004; Erwin, 2006; Retallack and Krull, 2006) are the primary proposed sources of sedimentary carbon for these scenarios.

Comparison of Data with Models

As predicted by all models, erosional features that could reflect carbonate dissolution have been observed primarily in shallow-water facies on carbonate platforms, rather than in outer shelf sections. Contrary to the upwelling model, however, microbial limestones containing crystal fans also tend to be localized in the shallowest settings, on carbonate platform tops (Kershaw et al., 2002; Lehrmann et al., 2003), immediately overlying potential dissolution surfaces. Carbonate precipitates have not been observed immediately overlying the P-T boundary in outer shelf settings. Thus, the predicted environmental separation of dissolution and precipitation under the upwelling and/or overturn models is not observed. Instead, available stratigraphic evidence indicates a separation of dissolution and precipitation in time rather than space, as predicted by the extinction-driven and sedimentary carbon-release models. However, the upwelling and sedimentary release scenarios are not necessarily mutually exclusive. Initial release of carbon to the atmosphere could have led to warming that triggered anoxia and the buildup of alkalinity, total CO_2, and hydrogen sulfide in the deep sea (Knoll et al., 1996; Hotinski et al., 2001; Beauchamp and Baud, 2002), followed by catastrophic upwelling of anoxic, high-alkalinity deep water to the sea surface (Grotzinger and Knoll, 1995; Knoll et al., 1996; Kershaw et al., 2002; Lehrmann et al., 2003). We prefer the upwelling and sedimentary release models to the extinction-driven model of Rampino and Caldeira (2005) because they provide a causal explanation for extinction as well as associated sedimentary and geochemical observations. We prefer the sedimentary release models to the upwelling models because they better account for the environmental and temporal relationships between truncation surfaces and microbialites containing carbonate fans. Of

the sedimentary release models, thermogenic methane production during Siberian Traps eruptions can better account for continuing large carbon isotope excursions during the 5 m.y. of the Early Triassic (Payne et al., 2004; Korte et al., 2005; Lehrmann et al., 2006), because the time scale for seafloor methane clathrate regeneration is too long to explain these features (Payne et al., 2004), and the initial release at the P-T boundary would have largely depleted the clathrate reservoir.

Could carbon release to the atmosphere occur with sufficient rapidity to cause widespread carbonate dissolution? A similar scenario is the favored explanation for the observed pattern of carbonate accumulation during the PETM event (Zachos et al., 2005). Numerical modeling indicates that the release of ~5×10^{18} g (5000 Gt) of carbon in less than a few thousand years would exceed the buffering capacity provided by dissolution of deep-sea carbonate sediment in the modern ocean (Archer et al., 1997). Caldeira and Wickett (2003) calculated a decrease in surface ocean pH by >0.7 units and deep-ocean pH by 0.4 units for oxidation of 5000 Gt carbon over time scales of <100 k.y., corresponding to a fivefold reduction in carbonate ion concentration. The concentration of Ca ions is conservative on these time scales and, therefore, the fivefold reduction in carbon ion concentration translates approximately to a fivefold reduction in carbonate saturation of seawater. Experiments demonstrate substantial sensitivity of many extant calcifying organisms to much more modest changes in seawater pH and carbonate saturation (e.g., Gattuso et al., 1998; Langdon et al., 2000; Riebesell et al., 2000). Although the Permian ocean may have contained a larger dissolved inorganic carbon reservoir (Rampino and Caldeira, 2005), it would have been less effectively buffered from CO_2 input by seafloor carbonate dissolution than the modern ocean due to the absence of pelagic calcifiers and associated deep-sea carbonate accumulations (Ridgwell and Zeebe, 2005). The Paleozoic and early Mesozoic carbonate compensation depth (CCD; the depth below which carbonate sediments are not preserved, today near 4000 m water depth) may also have been quite shallow (Jenkyns and Winterer, 1982; Malinky and Heckel, 1998) near the continental shelf-slope break, shoaling to continental shelf depths when inputs of alkalinity to the ocean waned or large inputs of carbon dioxide to the atmosphere occurred. Short-term buffering of CO_2 release (on time scales of ~10 k.y.) by carbonate dissolution could only have occurred in shallow shelf carbonates, which provide a less efficient buffer due to their more limited surface area (Archer et al., 1997). Thus, even release of <5000 Gt carbon could likely have caused an excursion of the CCD onto carbonate platforms and a substantial increase in atmospheric pCO_2. Partial restriction of water circulation on the shallow-marine carbonate platforms examined in this study may have enhanced the magnitude of dissolution at these localities if the time scale of significant change in atmospheric pCO_2 was shorter than the time scale of water mixing across the platforms. The silicate weathering feedback would have operated similarly to today, with ~200 k.y. required for silicate weathering and associated delivery of carbonate alkalinity to return the system to steady state (Archer et al., 1997), compatible with the estimated duration of microbialite deposition (Lehrmann et al., 2003).

It is important to distinguish the transient pulse in carbonate deposition driven by rapid release of carbon into the ocean-atmosphere system from longer-term changes in the steady-state carbonate saturation of seawater. The near absence of skeletal carbonate sinks through much of the Early Triassic (Payne et al., 2006) is likely to have caused a long-term shift in the carbonate saturation of seawater that can help to explain the persistence of large ooids, microbialites, flat-pebble conglomerates, and other carbonate facies more typical of Proterozoic and early Paleozoic strata (Pruss et al., 2005).

Comparison to the PETM suggests that the minimum carbon release required for shallow-marine carbonate dissolution at the P-T boundary is unusual, but not unprecedented. The severe biological consequences of the end-Permian event, however, suggest either a much larger carbon release or much greater sensitivity of the Earth system to carbon release at that time. The Late Permian marine biota contained a much higher proportion of taxa inferred to be sensitive to changes in pCO_2 and carbonate saturation (sensu Knoll et al., 1996) than does the modern ocean. However, end-Permian extinction rates were much higher than Paleocene-Eocene extinction rates, even among less sensitive taxa. The limited buffering capacity of the Late Permian oceans resulting from the absence of deep-sea carbonate sediments suggests that a similar carbon release would have had a much larger effect on the carbonate chemistry of Late Permian oceans.

At present, we prefer a model of extinction and carbonate dissolution driven by the release of sedimentary carbon to the atmosphere because it best accounts for the observation that microbialites universally postdate the truncation surface. The reduction in seawater carbonate saturation and briefly undersaturated conditions implied by petrographic observations would have potentially severe biological consequences. Ambient carbonate saturation exerts significant control on the rate (and mineralogy) of calcification in extant marine taxa (Gattuso et al., 1998; Marubini and Atkinson, 1999; Langdon et al., 2000; Riebesell et al., 2000; Ohde and Hossain, 2004). Taxa with heavy calcification and limited ability to buffer calcifying fluids from surrounding seawater are most vulnerable to rapid changes in ambient conditions, and genus-level extinction rates vary dramatically across higher taxa as a function of skeletal mineralogy and degree of calcification. Heavily calcified genera were most strongly affected, genera with phosphatic skeletons were least affected, and moderately to lightly calcified genera had intermediate extinction rates (Knoll et al., 1996, 2007). Thus, a combination of high pCO_2 and reduced seawater carbonate saturation may have acted synergistically in preferentially eliminating heavily calcified marine taxa with limited ability to compensate physiologically for rapid changes in the carbonate chemistry of surrounding seawater. This is not to say that other environmental stresses, especially anoxia and H_2S (Wignall and Hallam, 1992; Wignall and Twitchett, 1996; Kump et al., 2005), could not also have been important agents of extinction. Such stresses were no doubt present (Wignall and Twitchett, 2002; Grice et al., 2005), but must account more for the magnitude than the selectivity of marine extinctions (Knoll et al., 2007).

CONCLUSIONS

Evidence of shallow-marine carbonate dissolution across the extinction horizon followed by a pulse of rapid, postextinction carbonate precipitation suggests massive carbon release and extinction in <100 k.y., supporting the shorter end of time scales compatible with other geochronological and sedimentological data (Bowring et al., 1998; Rampino et al., 2000; Twitchett et al., 2001). Such a scenario can account for physiological selectivity of extinction (Knoll et al., 1996, 2007) through the combined effects of increased pCO_2 and $CaCO_3$ undersaturation of large areas of tropical oceans. Resultant shallow-marine anoxia and euxinia and H_2S release to the atmosphere may have enhanced the magnitude of extinction (Kajiwara et al., 1994; Wignall and Twitchett, 1996; Isozaki, 1997; Hotinski et al., 2001; Grice et al., 2005; Kump et al., 2005). Siberian Traps interactions with carbonates and coals of the Tugusskaya Series (Erwin, 2006), methane release from gas hydrates (Krull and Retallack, 2000), and bolide impact (Becker et al., 2001) into carbon-rich crustal strata could each account for carbon release, although continuing Siberian Traps magmatism (Ivanov et al., 2005) also provides an explanation for persistent Early Triassic carbon cycle instability

(Payne et al., 2004; Payne and Kump, 2007). Regardless of the source of carbon, however, associated effects on carbonate dissolution and/or precipitation indicate dramatic fluctuations in oceanic $CaCO_3$ saturation during and after marine extinctions. Whether the magnitude of extinction and associated changes in carbonate dissolution and/or precipitation primarily reflect the quantity of carbon released, the buffering capacity of the oceans, or the taxonomic and physiological composition of the marine fauna has yet to be determined. However, the lesser taxonomic and ecological severity of extinction associated with later episodes of massive carbon release (McElwain et al., 1999; Svensen et al., 2004) suggests that the magnitude of the end-Permian biodiversity crisis was contingent upon biological and geological contexts.

ACKNOWLEDGMENTS

We thank Y. Yu, J. Xiao, H. Yao, and A. Bush for assistance in the field and A. Airo, T. Beatty, S. Finnegan, A. Knoll, D. Lowe, M. Orchard, S. Pruss, and M. Tice for helpful comments and discussion. The manuscript was greatly improved by constructive reviews from B. Pratt, P. Wignall, A. Baud, and G. Retallack. This study was supported by the U.S. National Science Foundation (grants EAR-9804835 to Lehrmann, EAR-0208119 to Kump, and OCE-0084032 to A. Knoll, project EREUPT [Evolution and Radiation of Eukaryotic Phytoplankton]), the American Chemical Society (grant ACS-40948-B2 to Lehrmann), the U.S. National Aeronautical and Space Administration Astrobiology Institute (grants NCC2–0517 and NNA04CC06A to Kump), and a Sigma Xi Grant-in-Aid of Research to Payne.

REFERENCES CITED

Archer, D., Kheshgi, H., and Maier-Reimer, E., 1997, Multiple timescales for neutralization of fossil fuel CO2: Geophysical Research Letters, v. 24, p. 405–408, doi: 10.1029/97GL00168.

Baud, A., Magaritz, M., and Holser, W.T., 1989, Permian-Triassic of the Tethys—Carbon isotope studies: Geologische Rundschau, v. 78, p. 649–677, doi: 10.1007/BF01776196.

Baud, A., Cirilli, S., and Marcoux, J., 1997, Biotic response to mass extinction: The lowermost Triassic microbialites: Facies, v. 36, p. 238–242.

Baud, A., Richoz, S., and Marcoux, J., 2005, Calcimicrobial cap rocks from the basal Triassic units: Western Taurus occurrences (SW Turkey): Comptes Rendus Palevol, v. 4, p. 569–582, doi: 10.1016/j.crpv.2005.03.001.

Beauchamp, B., and Baud, A., 2002, Growth and demise of Permian biogenic chert along northwest Pangea: Evidence for end-Permian collapse of thermohaline circulation: Palaeogeography, Palaeoclimatology, Palaeoecology, v. 184, p. 37–63, doi: 10.1016/S0031-0182(02)00245-6.

Becker, L., Poreda, R.J., Hunt, A.G., Bunch, T.E., and Rampino, M., 2001, Impact event at the Permian-Triassic boundary: Evidence from extraterrestrial noble gases in fullerenes: Science, v. 291, p. 1530–1533, doi: 10.1126/science.1057243.

Bowring, S.A., Erwin, D.H., Jin, Y.G., Martin, M.W., Davidek, K., and Wang, W., 1998, U/Pb zircon geochronology and tempo of the end-Permian mass extinction: Science, v. 280, p. 1039–1045, doi: 10.1126/science.280.5366.1039.

Broecker, W.S., and Peng, T.-H., 1982, Tracers in the Sea: Palisades, New York, Eldigo Press, 690 p.

Caldeira, K., and Wickett, M.E., 2003, Anthropogenic carbon and ocean pH: Nature, v. 425, p. 365–365, doi: 10.1038/425365a.

Cao, C., and Shang, Q., 1998, Microstratigraphy of Permo-Triassic transitional sequence of the Meishan section, Zhejiang, China: Palaeoworld, v. 9, p. 147–152.

Crasquin-Soleau, S., Richoz, S., Marcoux, J., Angiolini, L., Nicora, A., and Baud, A., 2002, The events of the Permian-Trias boundary: Last survivors and/or first colonisers among the ostracods of the Thurides (southwestern Turkey): Comptes Rendus Geoscience, v. 334, p. 489–495, doi: 10.1016/S1631-0713(02)01782-0.

Enos, P., 1995, Permian in China, *in* Scholle, P.A., et al., eds., The Permian of northern Pangea: Berlin, Springer-Verlag, p. 225–256.

Erwin, D.H., 2006, Extinction: How life on Earth nearly ended 250 million years ago: Princeton, New Jersey, Princeton University Press, 306 p.

Ezaki, Y., and Yao, A., 2000, Permian–Triassic successions in Japan: Key to deciphering Permian/Triassic events, *in* Yin, H.F., et al., eds., Permo-Triassic evolution of Tethys, Circum-Pacific and marginal Gondwana: Amsterdam, Elsevier, p. 127–139.

Ezaki, Y., Liu, J.B., and Adachi, N., 2003, Earliest Triassic microbialite micro- to megastructures in the Huaying area of Sichuan Province, South China: Implications for the nature of oceanic conditions after the end-Permian extinction: Palaios, v. 18, p. 388–402.

Flügel, E., 2002, Triassic reef patterns, *in* Kiessling, et al., eds., Phanerozoic reef patterns: SEPM (Society for Sedimentary Geology) Special Publication 72, p. 391–464.

Flügel, E., 2004, Microfacies of carbonate rocks: Berlin, Springer, 976 p.

Gattuso, J.P., Frankignoulle, M., Bourge, I., Romaine, S., and Buddemeier, R.W., 1998, Effect of calcium carbonate saturation of seawater on coral calcification: Global and Planetary Change, v. 18, p. 37–46, doi: 10.1016/S0921-8181(98)00035-6.

Grice, K., Cao, C.Q., Love, G.D., Bottcher, M.E., Twitchett, R.J., Grosjean, E., Summons, R.E., Turgeon, S.C., Dunning, W., and Jin, Y.G., 2005, Photic zone euxinia during the Permian-Triassic superanoxic event: Science, v. 307, p. 706–709, doi: 10.1126/science.1104323.

Grotzinger, J.P., and Knoll, A.H., 1995, Anomalous carbonate precipitates: Is the Precambrian the key to the Permian?: Palaios, v. 10, p. 578–596, doi: 10.2307/3515096.

Groves, J.R., and Calner, M., 2004, Lower Triassic oolites in Tethys: A sedimentologic response to the end-Permian mass extinction: Geological Society of America Abstracts with Programs, v. 36, no. 5, p. 336.

Groves, J.R., Altiner, D., and Rettori, R., 2005, Extinction, survival, and recovery of lagenide foraminifers in the Permian-Triassic boundary interval, central Taurides, Turkey: Journal of Paleontology Memoir, v. 62, p. 1–38.

Haas, J., Demény, A., Hips, K., and Vennemann, T., 2006, Carbon isotope excursions and microfacies changes in marine Permian-Triassic boundary sections in Hungary: Palaeogeography, Palaeoclimatology, Palaeoecology, v. 237, p. 160–181, doi: 10.1016/j.palaeo.2005.11.017.

Heydari, E., and Hassanzadeh, J., 2003, Deev Jahi model of the Permian-Triassic boundary mass extinction: A case for gas hydrates as the main cause of biological crisis on Earth: Sedimentary Geology, v. 163, p. 147–163, doi: 10.1016/j.sedgeo.2003.08.002.

Heydari, E., Wade, W.J., and Hassanzadeh, J., 2001, Diagenetic origin of carbon and oxygen isotope compositions of Permian-Triassic boundary strata: Sedimentary Geology, v. 143, p. 191–197, doi: 10.1016/S0037-0738(01)00095-1.

Heydari, E., Hassanzadeh, J., Wade, W.J., and Ghazi, A.M., 2003, Permian-Triassic boundary interval in the Abadeh section of Iran with implications for mass extinction: Part 1—Sedimentology: Palaeogeography, Palaeoclimatology, Palaeoecology, v. 193, p. 405–423, doi: 10.1016/S0031-0182(03)00258-X.

Hillgartner, H., 1998, Discontinuity surfaces on a shallow-marine carbonate platform (Berriasian, Valanginian, France and Switzerland): Journal of Sedimentary Research, v. 68, p. 1093–1108.

Holland, S.M., 1995, The stratigraphic distribution of fossils: Paleobiology, v. 21, p. 92–109.

Hotinski, R.M., Bice, K.L., Kump, L.R., Najjar, R.G., and Arthur, M.A., 2001, Ocean stagnation and end-Permian anoxia: Geology, v. 29, p. 7–10, doi: 10.1130/0091-7613(2001)029<0007:OSAEPA>2.0.CO;2.

Immenhauser, A., Schlager, W., Burns, S.J., Scott, R.W., Geel, T., Lehmann, J., Van der Gaast, S., and Bolder-Schrijver, L.J.A., 1999, Late Aptian to late Albian sea-level fluctuations constrained by geochemical and biological evidence (Nahr Umr formation, Oman): Journal of Sedimentary Research, v. 69, p. 434–446.

Isozaki, Y., 1997, Timing of Permian-Triassic anoxia: Science, v. 277, p. 1748–1749.

Ivanov, A.V., Rasskazov, S.V., Feoktistov, G.D., He, H., and Boven, A., 2005, $^{40}Ar/^{39}Ar$ dating of Usol'skii sill in the south-eastern Siberian Traps large igneous province: Evidence for long-lived magmatism: Terra Nova, v. 17, p. 203–208, doi: 10.1111/j.1365-3121.2004.00588.x.

Jenkyns, H.C., and Winterer, E.L., 1982, Palaeoceanography of Mesozoic ribbon radiolarites: Earth and Planetary Science Letters, v. 60, p. 351–375, doi: 10.1016/0012-821X(82)90073-5.

Jiang, H., Lai, X., Luo, G., Aldridge, R., Zhang, K., and Wignall, P., 2007, Restudy of conodont zonation and evolution across the P/T boundary at Meishan section, Changxing, Zhejiang, China: Global and Planetary Change, v. 55, p. 39–55, doi: 10.1016/j.gloplacha.2006.06.007.

Jin, Y.G., Wang, Y., Wang, W., Shang, Q.H., Cao, C.Q., and Erwin, D.H., 2000, Pattern of marine mass extinction near the Permian-Triassic boundary in South China: Science, v. 289, p. 432–436, doi: 10.1126/science.289.5478.432.

Kajiwara, Y., Yamakita, S., Ishida, K., Ishiga, H., and Imai, A., 1994, Development of a largely anoxic stratified ocean and its temporary massive mixing at the Permian-Triassic boundary supported by the sulfur isotopic record: Palaeogeography, Palaeoclimatology, Palaeoecology, v. 111, p. 367–379, doi: 10.1016/0031-0182(94)90072-8.

Kanmera, K., and Nakazawa, K., 1973, Permian-Triassic relationship and faunal changes in the eastern Tethys, *in* Logan, A., and Hills, L.V., eds., The Permian and Triassic Systems and their mutual boundary: Canadian Society of Petroleum Geologists Memoir 2, p. 100–119.

Kershaw, S., Zhang, T.S., and Lan, G.Z., 1999, A?microbialite carbonate crust at the Permian-Triassic boundary in South China, and its palaeoenvironmental significance: Palaeogeography, Palaeoclimatology, Palaeoecology, v. 146, p. 1–18, doi: 10.1016/S0031-0182(98)00139-4.

Kershaw, S., Guo, L., Swift, A., and Fan, J.S., 2002, Microbialites in the Permian-Triassic boundary interval in central China: Structure, age and distribution: Facies, v. 47, p. 83–89.

Knoll, A.H., Bambach, R.K., Canfield, D.E., and Grotzinger, J.P., 1996, Comparative Earth history and Late Permian mass extinction: Science, v. 273, p. 452–457, doi: 10.1126/science.273.5274.452.

Knoll, A.H., Bambach, R.K., Payne, J.L., Pruss, S., and Fischer, W.W., 2007, Paleophysiology and end-Permian mass extinction: Earth and Planetary Science Letters, v. 256, p. 295–313, doi:10.1016/j.epsl.2007.02.018.

Koike, T., 1996, The first occurrence of Griesbachian conodonts in Japan: Palaeontological Society of Japan Transactions and Proceedings, new series, v. 181, p. 337–346.

Korte, C., Kozur, H.W., and Veizer, J., 2005, $\delta^{13}C$ and $\delta^{18}O$ values of Triassic brachiopods and carbonate rocks as proxies for coeval seawater and palaeotemperature: Palaeogeography, Palaeoclimatology, Palaeoecology, v. 226, p. 287–306, doi: 10.1016/j.palaeo.2005.05.018.

Krull, E.S., and Retallack, G.J., 2000, $\delta^{13}C$ depth profiles from paleosols across the Permian-Triassic boundary: Evidence for methane release: Geological Society of America Bulletin, v. 112, p. 1459–1472, doi: 10.1130/0016-7606(2000)112<1459:CDPFPA>2.0.CO;2.

Krull, E.S., Lehrmann, D.J., Druke, D., Kessel, B., Yu, Y.Y., and Li, R.X., 2004, Stable carbon isotope stratigraphy across the Permian-Triassic boundary in shallow marine carbonate platforms, Nanpanjiang Basin, south China: Palaeo-

geography, Palaeoclimatology, Palaeoecology, v. 204, p. 297–315, doi: 10.1016/S0031-0182(03)00732-6.

Kump, L.R., Pavlov, A., and Arthur, M.A., 2005, Massive release of hydrogen sulfide to the surface ocean and atmosphere during intervals of oceanic anoxia: Geology, v. 33, p. 397–400, doi: 10.1130/G21295.1.

Langdon, C., Takahashi, T., Sweeney, C., Chipman, D., Goddard, J., Marubini, F., Aceves, H., Barnett, H., and Atkinson, M.J., 2000, Effect of calcium carbonate saturation state on the calcification rate of an experimental coral reef: Global Biogeochemical Cycles, v. 14, p. 639–654, doi: 10.1029/1999GB001195.

Lehrmann, D.J., 1999, Early Triassic calcimicrobial mounds and biostromes of the Nanpanjiang basin, south China: Geology, v. 27, p. 359–362, doi: 10.1130/0091-7613(1999)027<0359:ETCMAB>2.3.CO;2.

Lehrmann, D.J., Wei, J.Y., and Enos, P., 1998, Controls on facies architecture of a large Triassic carbonate platform: The Great Bank of Guizhou, Nanpanjiang Basin, South China: Journal of Sedimentary Research, v. 68, p. 311–326.

Lehrmann, D.J., Wan, Y., Wei, J.Y., Yu, Y.Y., and Xiao, J.F., 2001, Lower Triassic peritidal cyclic limestone: An example of anachronistic carbonate facies from the Great Bank of Guizhou, Nanpanjiang Basin, Guizhou Province: South China: Palaeogeography, Palaeoclimatology, Palaeoecology, v. 173, p. 103–123, doi: 10.1016/S0031-0182(01)00302-9.

Lehrmann, D.J., Payne, J.L., Felix, S.V., Dillett, P.M., Wang, H., Yu, Y.Y., and Wei, J.Y., 2003, Permian-Triassic boundary sections from shallow-marine carbonate platforms of the Nanpanjiang Basin, south China: Implications for oceanic conditions associated with the end-Permian extinction and its aftermath: Palaios, v. 18, p. 138–152.

Lehrmann, D.J., Ramezani, J., Martin, M.W., Bowring, S.A., Montgomery, P., Enos, P., Payne, J.L., Orchard, M.J., Wang, H.-M., and Wei, J., 2006, Timing of biotic recovery from the end-Permian extinction: Biostratigraphic and geochronologic constraints from south China: Geology, v. 34, p. 1053–1056, doi: 10.1130/G22827A.1.

Lehrmann, D.J., Payne, J.L., Pei, D., Enos, P., Ellwood, B., Orchard, M.J., Zhang, J., and Wei, J., 2007, Record of the end-Permian extinction and Triassic biotic recovery in the Chongzuo-Pingguo Platform, southern Nanpanjiang Basin, Guangxi, south China: Palaeogeography, Palaeoclimatology, Palaeoecology, doi:10.1016/j.palaeo.2006.11.044 (in press).

Malinky, J.M., and Heckel, P.H., 1998, Paleoecology and taphonomy of faunal assemblages in gray "core" (offshore) shales in midcontinent Pennsylvanian cyclothems: Palaios, v. 13, p. 311–334, doi: 10.2307/3515321.

Marcoux, J., and Baud, A., 1986, The Permo-Triassic boundary in the Antalya Nappes (western Taurides, Turkey): Memorie della Società Geologica Italiana, v. 34, p. 243–252.

Marubini, F., and Atkinson, M.J., 1999, Effects of lowered pH and elevated nitrate on coral calcification: Marine Ecology Progress Series, v. 188, p. 117–121.

McElwain, J.C., Beerling, D.J., and Woodward, F.I., 1999, Fossil plants and global warming at the Triassic-Jurassic boundary: Science, v. 285, p. 1386–1390, doi: 10.1126/science.285.5432.1386.

Monod, O., 1977, Recherches géologiques dans le Taurus occidental au Sud de Beysehir (Turquie) [Ph.D. thesis]: Université de Paris-Sud, Centre d'Orsay, 442 p.

MTA (General Directorate of Mineral Research and Exploration), 2002, Geological map of Turkey. Konya sheet: Ankara, General Directorate of Mineral Research and Exploration, scale 1:500 000.

Musashi, M., Isozaki, Y., Koike, T., and Kreulen, R., 2001, Stable carbon isotope signature in mid-Panthalassa shallow-water carbonates across the Permo-Triassic boundary: Evidence for C-13-depleted superocean: Earth and Planetary Science Letters, v. 191, p. 9–20, doi: 10.1016/S0012-821X(01)00398-3.

Ohde, S., and Hossain, M.M.M., 2004, Effect of $CaCO_3$ (aragonite) saturation state of seawater on calcification of *Porites* coral: Geochemical Journal, v. 38, p. 613–621.

Özgül, N., 1997, Stratigraphy of the tectono-stratigraphic units in the region Bozkir-Hadim-Taşkent (northern central Taurides) [in Turkish with English abstract]: Mineral Research and Exploration Institute of Turkey (MTA) Bulletin, v. 119, p. 113–174.

Payne, J.L., and Kump, L.R., 2007, Evidence for recurrent Early Triassic massive volcanism from quantitative interpretation of carbon isotope fluctuations: Earth and Planetary Science Letters, v. 256, p. 264–277, doi:10.1016/j.epsl.2007.01.034.

Payne, J.L., Lehrmann, D.J., Wei, J.Y., Orchard, M.J., Schrag, D.P., and Knoll, A.H., 2004, Large perturbations of the carbon cycle during recovery from the end-Permian extinction: Science, v. 305, p. 506–509, doi: 10.1126/science.1097023.

Payne, J.L., Lehrmann, D.J., Wei, J., and Knoll, A.H., 2006, The pattern and timing of biotic recovery from the end-Permian extinction on the Great Bank of Guizhou, Guizhou Province, China: Palaios, v. 21, p. 63–85, doi: 10.2110/palo.2005.p05-12p.

Pruss, S.B., Corsetti, F.A., and Bottjer, D.J., 2005, The unusual sedimentary rock record of the Early Triassic: A case study from the southwestern United States: Palaeogeography, Palaeoclimatology, Palaeoecology, v. 222, p. 33–52, doi: 10.1016/j.palaeo.2005.03.007.

Rampino, M.R., and Caldeira, K., 2005, Major perturbation of ocean chemistry and a 'Strangelove Ocean' after the end-Permian mass extinction: Terra Nova, v. 17, p. 554–559, doi: 10.1111/j.1365-3121.2005.00648.x.

Rampino, M.R., Prokoph, A., and Adler, A., 2000, Tempo of the end-Permian event: High-resolution cyclostratigraphy at the Permian-Triassic boundary: Geology, v. 28, p. 643–646, doi: 10.1130/0091-7613(2000)28<643:TOTEEH>2.0.CO;2.

Retallack, G.J., 1999, Postapocalyptic greenhouse paleoclimate revealed by earliest Triassic paleosols in the Sydney Basin, Australia: Geological Society of America Bulletin, v. 111, p. 52–70, doi: 10.1130/0016-7606(1999)111<0052:PGPRBE>2.3.CO;2.

Retallack, G.J., and Krull, E.S., 2006, Carbon isotopic evidence for terminal-Permian methane outbursts and their role in extinctions of animals, plants, coral reefs, and peat swamps, *in* Greb, S.F., and DiMichele, W.A., eds., Wetlands through time: Geological Society of America Special Paper 399, p. 249–268.

Retallack, G.J., Veevers, J.J., and Morante, R., 1996, Global coal gap between Permian-Triassic extinction and Middle Triassic recovery of peat-forming plants: Geological Society of America Bulletin, v. 108, p. 195–207, doi: 10.1130/0016-7606(1996)108<0195:GCGBPT>2.3.CO;2.

Richoz, S., 2004, Stratigraphie et variations isotopiques due carbone dans le Permien supérieur et le Trias inférieur de la Néotéthys (Turquie, Oman et Iran): Lausanne, Switzerland, Université de Lausanne, 251 p.

Ridgwell, A., and Zeebe, R.E., 2005, The role of the global carbonate cycle in the regulation and evolution of the Earth system: Earth and Planetary Science Letters, v. 234, p. 299–315, doi: 10.1016/j.epsl.2005.03.006.

Riebesell, U., Zondervan, I., Rost, B., Tortell, P.D., Zeebe, R.E., and Morel, F.M.M., 2000, Reduced calcification in marine plankton in response to increased atmospheric CO_2: Nature, v. 407, p. 634–637.

Sano, H., and Nakashima, K., 1997, Lowermost Triassic (Griesbachian) microbial bindstone-cementstone facies, southwest Japan: Facies, v. 36, p. 1–24, doi: 10.1007/BF02536874.

Sattler, U., Immenhauser, A., Hillgartner, H., and Esteban, M., 2005, Characterization, lateral variability and lateral extent of discontinuity surfaces on a carbonate platform (Barremian to Lower Aptian, Oman): Sedimentology, v. 52, p. 339–361, doi: 10.1111/j.1365-3091.2005.00701.x.

Schubert, J.K., and Bottjer, D.J., 1992, Early Triassic stromatolites as post mass extinction disaster forms: Geology, v. 20, p. 883–886, doi: 10.1130/0091-7613(1992)020<0883:ETSAPM>2.3.CO;2.

Scotese, C.R., 2005, Early Triassic paleogeographic map: http://www.scotese.com/newpage8.htm (accessed January 2007).

Sheldon, N.D., 2006, Abrupt chemical weathering increase across the Permian-Triassic boundary: Palaeogeography, Palaeoclimatology, Palaeoecology, v. 231, p. 315–321, doi: 10.1016/j.palaeo.2005.09.001.

Signor, P.W., and Lipps, J.H., 1982, Sampling bias, gradual extinction patterns, and catastrophes in the fossil record, *in* Silver, L.T., and Schultz, P.H., eds., Geological implications of impacts of large asteroids and comets on the Earth: Geological Society of America Special Paper 190, p. 291–296.

Svensen, H., Planke, S., Malthe-Sorenssen, A., Jamtveit, B., Myklebust, R., Eidem, T.R., and Rey, S.S., 2004, Release of methane from a volcanic basin as a mechanism for initial Eocene global warming: Nature, v. 429, p. 542–545, doi: 10.1038/nature02566.

Twitchett, R.J., Looy, C.V., Morante, R., Visscher, H., and Wignall, P.B., 2001, Rapid and synchronous collapse of marine and terrestrial ecosystems during the end-Permian biotic crisis: Geology, v. 29, p. 351–354, doi: 10.1130/0091-7613(2001)029<0351:RASCOM>2.0.CO;2.

Unal, E., Altiner, D., Yilmaz, I.O., and Ozkan-Altiner, S., 2003, Cyclic sedimentation across the Permian-Triassic boundary (Central Taurides, Turkey): Rivista Italiana di Paleontologia e Stratigrafia, v. 109, p. 359–376.

Wang, Y.B., Tong, J.N., Wang, J.S., and Zhou, X.G., 2005, Calcimicrobialite after end-Permian mass extinction in South China and its paleoenvironmental significance: Chinese Science Bulletin, v. 50, p. 665–671, doi: 10.1360/982004-323.

Ward, P.D., Montgomery, D.R., and Smith, R., 2000, Altered river morphology in South Africa related to the Permian-Triassic extinction: Science, v. 289, p. 1740–1743, doi: 10.1126/science.289.5485.1740.

Webb, G.E., 1996, Was Phanerozoic reef history controlled by the distribution of non-enzymatically secreted reef carbonates (microbial carbonate and biologically induced cement)?: Sedimentology, v. 43, p. 947–971, doi: 10.1111/j.1365-3091.1996.tb01513.x.

Wignall, P.B., and Hallam, A., 1992, Anoxia as a cause of the Permian Triassic mass extinction: Facies evidence from northern Italy and the western United-States: Palaeogeography, Palaeoclimatology, Palaeoecology, v. 93, p. 21–46, doi: 10.1016/0031-0182(92)90182-5.

Wignall, P.B., and Twitchett, R.J., 1996, Oceanic anoxia and the end Permian mass extinction: Science, v. 272, p. 1155–1158, doi: 10.1126/science.272.5265.1155.

Wignall, P.B., and Twitchett, R.J., 2002, Extent, duration, and nature of the Permian-Triassic superanoxic event, *in* Koeberl, C., and MacLeod, K.G., eds., Catastrophic events and mass extinctions; impacts and beyond: Geological Society of America Special Paper 356, p. 395–413.

Woods, A.D., Bottjer, D.J., Mutti, M., and Morrison, J., 1999, Lower Triassic large sea-floor carbonate cements: Their origin and a mechanism for the prolonged biotic recovery from the end-Permian mass extinction: Geology, v. 27, p. 645–648, doi: 10.1130/0091-7613(1999)027<0645:LTLSFC>2.3.CO;2.

Yin, H., Zhang, K., Tong, J., Yang, Z., and Wu, S., 2001, The global stratotype section and point (GSSP) of the Permian-Triassic boundary, *in* International Symposium on the Global Stratotype of the Permian-Triassic Boundary and the Paleozoic-Mesozoic Events, Changxing, China: Changxing, China, China University of Geosciences, China Geological Survey, Nanjing Institute of Geology and Palaeontology, Chinese Academy of Sciences, and the Government of Changxing County, Zhejiang Province p. 1–12.

Zachos, J.C., Rohl, U., Schellenberg, S.A., Sluijs, A., Hodell, D.A., Kelly, D.C., Thomas, E., Nicolo, M., Raffi, I., Lourens, L.J., McCarren, H., and Kroon, D., 2005, Rapid acidification of the ocean during the Paleocene-Eocene thermal maximum: Science, v. 308, p. 1611–1615, doi: 10.1126/science.1109004.

Manuscript Received 16 August 2006
Revised Manuscript Received 19 February 2007
Manuscript Accepted 7 March 2007

Printed in the USA